Online Supporting Information (SI) for "Correction methods for first-principles calculations of the solution enthalpy of gases and compounds in liquid metals"

Appendix

A. Detailed explanation of enthalpy diagram

Fig. 1 in the main body is the enthalpy diagram for the solution enthalpy calculation in this study. This Appendix describes how the differences in the enthalpies between the levels in the diagram were obtained from the first-principles calculation results, by clarifying the state of each enthalpy level, and explains the correspondence between the left-hand side and the right-hand side of the diagram.

A.1. Clarification of state of each enthalpy level[1]

$\Delta H_{f,Na_iX(s)}^{600\,K}$ indicates the standard formation enthalpy of a solid Na-impurity compound, $Na_iX\,(s)$, at 600 K. Here, X represents an impurity element in liquid Na, e.g., H, N, O, and I, and i represents a stoichiometric number for Na in a solid sodium compound, e.g., 1 in NaH and 2 in Na_2O. As shown in Fig. A1, the sum of (i) the FPMD result of pure liquid Na (per 102 Na atoms) at 600 K, multiplied by i/102, and (ii) the vibration analysis result of a gas X_2 molecule (per X_2 molecule) at 600 K, multiplied by 1/2, was subtracted from the Debye model result of solid Na_iX (per unit of i Na atoms and 1 impurity atom) at 600 K.

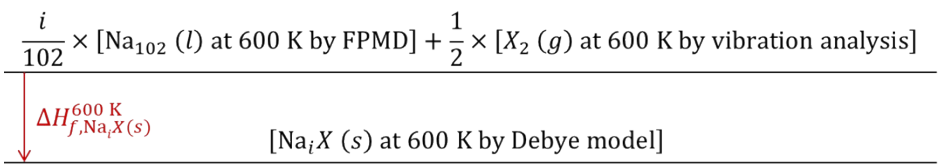

Figure A1. Derivation of $\Delta H_{f,Na_iX(s)}^{600\,K}$ from first-principles calculation results.

$\Delta H_{sol,X_2(g)}^{600K}$ indicates the solution enthalpy of X_2 (g) in liquid Na at 600 K. As shown in Fig. A2, the sum of (i) the FPMD result of pure liquid Na (per 102 Na atoms) at 600 K, multiplied by 101/102, and (ii) the vibration analysis result of a gas X_2 molecule (per X_2 molecule) at 600 K, multiplied by 1/2, was subtracted from the FPMD result of impurity-including liquid Na (per unit of 101 Na atoms and 1 impurity atom) at 600 K.

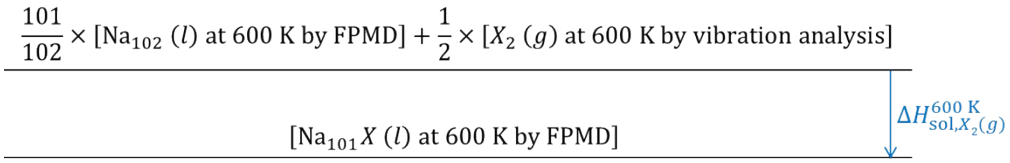

Figure A2. Derivation of $\Delta H^{600\ K}_{sol,X_2(g)}$ from first-principles calculation results.

$\Delta H^{600\ K}_{sol,Na_iX(s)}$ indicates the solution enthalpy of Na_iX (s) in liquid Na at 600 K. As shown in Fig. A3, the sum of (i) the FPMD result of pure liquid Na (per 102 Na atoms) at 600 K, multiplied by (101-i)/102, and (ii) the Debye model result of solid Na_iX (per unit of i Na atoms and 1 impurity atom) at 600 K was subtracted from the FPMD result of impurity-including liquid Na (per unit of 101 Na atoms and 1 impurity atom) at 600 K.

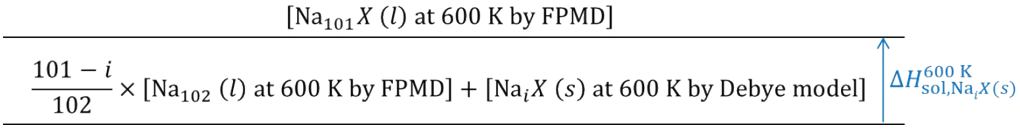

Figure A3. Derivation of $\Delta H^{600\ K}_{sol,Na_iX(s)}$ from first-principles calculation results.

A.2. Correspondence between left-hand side and right-hand side[1]

First, for the solid and dotted lines at the top, the correspondence is clear because only the number of liquid Na is changed from i to m.

For the solid and dotted lines at the bottom, the solid-liquid interfacial energy of Na_iX (s) in liquid Na is neglected. Accordingly, the enthalpy level represented by the dotted line, labeled [(m-i) Na (l) including Na_iX (s)], is equal to the sum of the enthalpies of pure liquid Na and solid Na_iX, namely, (m-i) [Na (l)] + [Na_iX (s)]. As mentioned in Section 2.1 of the main body, this treatment is similar to what is usually adopted in experiments to determine the solubility limit. With this treatment, the difference between the solid and dotted lines at the bottom is equal to (m-i) [Na (l)]. Thus, the difference between the solid lines at the top and at the bottom is equal to the difference between the corresponding dotted lines.

For the dotted line labeled [m Na (l) including X (impurity)], where m is a sufficiently large number, it is assumed that an impurity atom is sufficiently isolated in liquid Na so that no significant interaction occurs among the impurity atoms. This assumption is reasonable in experiments because (i) attractive interaction is not expected between the impurity atoms of the same element as they are negatively charged in liquid Na due to the large difference in the electronegativity between Na and impurity (Na: 0.93, H: 2.20, N: 3.04, O: 3.44, I: 2.66)[2] and (ii) the impurity concentration is basically low enough to regard that an accidental

encounter of two or more impurity atoms is not frequent. Indeed, the saturation concentrations of H, N, O, and I impurities in liquid Na are all less than 0.1% at 600 K according to the experimental data on the solubility limit.[3] Hence, we consider that the dissolution of X_2 (g) and Na_iX (s) in liquid Na are virtually independent of the impurity concentration unless the experimental conditions are extreme.

B. Settings and procedures for the first-principles calculations

B.1. Pure liquid Na (FPMD simulation)

A cubic simulation cell consisting of 102 Na atoms was prepared with the volume estimated to result in a zero pressure,[4] which is virtually equivalent to the atmospheric pressure for the simulations of condensed matter. The initial atomic configurations were brought from the FPMD simulations of LBE in our previous study.[5] The FPMD simulations were performed at 600 K for 25 ps with a time step of 1.6 fs. The break condition for the electronic self-consistent loop was set as the total free energy change between two steps smaller than 10^{-6} eV. A canonical (NVT) ensemble was simulated using a Nosé thermostat[6] as a temperature controlling method except for the first 1000 time steps where the velocities were scaled every time step to adjust the kinetic energy to 600 K for quick equilibration. The initial 5-ps data was discarded as equilibration calculations, and the remaining 20-ps data was used for the analysis. To improve the statistics for the liquid system, three independent FPMD simulations were performed with different initial atomic configurations. Thus, 60-ps data was analyzed in total.

In addition, six different cell constants, namely, 99.0%, 99.3%, 99.65%, 100.35%, 100.7%, and 101.0% of the initial cell constant, were used together with the initial cell constant to obtain the pressure-energy relationship for pure Na. A zero-pressure energy was estimated as an y-intercept of the second-order polynomial fit for the seven pressure-energy data points, with its standard deviation numerically estimated by using the Monte Carlo method described in our previous study.[1] Finally, from the definition of enthalpy, $H = E + PV$, the product of the atmospheric pressure (101325 Pa) and the system volume (~4400 Å^3), 0.0028 eV, was added to the zero-pressure energy to obtain the enthalpy of pure liquid Na at 600 K.

B.2. Impurity-including liquid Na (FPMD simulation)

One Na atom in the pure liquid Na system was randomly picked and replaced to an impurity atom. For this impurity-including liquid Na system, the FPMD simulation was performed at 600 K The initial 5-ps data was discarded as equilibration calculations, and the remaining 25-ps data was used for the analysis. To improve the statistics for the liquid system, two independent FPMD simulations were performed with

different initial atomic configurations. Thus, 50-ps data was analyzed in total for each impurity case.

The calculation cost is too high to obtain the pressure-energy relationship of impurity-including liquid Na for all impurities. Thus, it was assumed that the pressure-volume and pressure-energy relationships of pure liquid Na were similar to those of impurity-including liquid Na. This assumption is reasonable because only one of 102 Na atoms was replaced to an impurity atom, which is not expected to change significantly the pressure-volume and pressure-energy relationships of the whole system.

Before the main FPMD simulation of each impurity case, a 5-ps test FPMD simulation was performed with the initial cell constant used for pure Na. Next, from the system pressure averaged over 5 ps, a cell constant resulting in a zero pressure was estimated by using the pressure-volume relationship of pure Na. Then, the 30-ps main FPMD simulation was performed with the estimated cell constant for each impurity case. From the system energy and pressure averaged over 25 ps, a system energy resulting in a zero pressure was estimated by using the pressure-energy relationship of pure Na. Finally, the product of the atmospheric pressure (101325 Pa) and the system volume (~4400 Å^3), 0.0028 eV, was added to the zero-pressure energy to obtain the enthalpy of impurity-including liquid Na at 600 K.

B.3. Impurity gas molecule (vibration analysis)[1]

The enthalpy of an impurity gas molecule at 600 K needs to be obtained to calculate its solution enthalpy at 600 K. In this study, the impurity gas molecules were assumed to be ideal gases because we are interested in a system where the pressure is not very high and the temperature is not very low, which is a typical condition in the experiment. According to statistical thermodynamics,[7] thermodynamic quantities can be obtained from the partition function Z, which is written for an ideal gas molecule as

$$Z(N,V,T) = \frac{\left[q(V,T)\right]^N}{N!} \quad \text{(B1)}$$
$$q(V,T) = q_{trans} q_{rot} q_{vib} q_{elec}$$

where N is the number of molecules in the system, V (m^3) is the volume of the system, T (K) is the temperature of the system, and q is the partition function of a gas molecule with q_{trans}, q_{rot}, q_{vib} and q_{elec} being translational, rotational, vibrational and electronic components, respectively. For a diatomic gas molecule, the components of the partition function in Eq. (B1) is expressed as

$$
\begin{aligned}
&q_{trans}(V,T)=\left(\frac{2\pi m}{h^2\beta}\right)^{3/2}V \\
&q_{rot}(T)=\frac{T}{\Theta_{rot}}=\frac{8\pi^2 I}{h^2\beta},\ \Theta_{rot}=\frac{h^2}{8\pi^2 I k_B},\ I=\mu r_e^{\,2} \\
&q_{vib}=\sum_n e^{-\beta\varepsilon_n}=\sum_n e^{-\beta h\nu_n} \\
&q_{elec}=\sum_n g_{n,elec}e^{-\beta\varepsilon_{n,\mathrm{elec}}}=e^{D_e/k_BT} \\
&\beta=\frac{1}{k_BT}
\end{aligned}
\qquad \text{(B2)}
$$

where m (kg) is the mass of the molecule, Θ_{rot} (K) is the rotational temperature, I is the moment of inertia (kg·m^2), h is the Planck constant (6.62×10^{-34} J·s), μ (kg) is the reduced mass, which is equal to $0.5m$ in the case of a homonuclear diatomic molecule, r_e (m) is the bond distance, ε_n (J) is the n-th vibrational energy level, ν_n (Hz) is the vibration frequency of the n-th vibrational mode, $g_{n,elec}$ is the degeneracy of the n-th electronic energy level, $\varepsilon_{n,elec}$ (J) is the n-th electronic energy level, D_e (J) is the binding energy of the molecule, and k_B is the Boltzmann constant (1.38×10^{-23} J/K).

From Eq. (B2), the internal energy U (J/mol) is written as the sum of the partial derivatives of the partition function components, q_{trans}, q_{rot}, q_{vib} and q_{elec} (in order), which is

$$
\begin{aligned}
&U=-\frac{\partial}{\partial\beta}(\ln Z)=\left\{\frac{3}{2}Nk_BT\right\}+\left\{Nk_BT\right\}+\left\{N\frac{\sum_n\left(-\varepsilon_n e^{-\beta\varepsilon_n}\right)}{\sum_n e^{-\beta\varepsilon_n}}\right\}+\left\{-ND_e\right\} \\
&\beta=\frac{1}{k_BT}
\end{aligned}
\qquad \text{(B3)}
$$

In this study, the harmonic approximation was applied to the molecular vibration to simplify the calculation,[1] which rewrites Eq. (B3) as

$$
\begin{aligned}
&U_{\mathrm{harmonic}}=\left\{\frac{3}{2}Nk_BT\right\}+\left\{Nk_BT\right\}+\left\{Nk_B\left[\frac{\Theta_{vib}}{2}+\frac{\Theta_{vib}e^{-\Theta_{vib}/T}}{1-e^{-\Theta_{vib}/T}}\right]\right\}+\left\{-ND_e\right\} \\
&\Theta_{vib}=\frac{h\nu_h}{k_B}
\end{aligned}
\qquad \text{(B4)}
$$

where Θ_{vib} (K) is the vibrational temperature and ν_h (Hz) is the vibrational frequency of a harmonic oscillator.

Finally, using the fundamental relationship for thermodynamic quantities, enthalpy H (J/mol) was evaluated as

$$H = U + P\bar{V},\ \bar{V} = \frac{RT}{P} \quad \text{(B5)}$$

where R is the gas constant (8.31 J/K/mol) and P (Pa) is the pressure of the system.

In this study, a geometry optimization calculation was performed to determine the binding energy and the bond length of the impurity gas molecule. Based on the binding energy expressed as a function of a bond length, a 1D Schrödinger equation was solved under the harmonic approximation to obtain the vibrational frequency and the corresponding energy levels of the molecule. Finally, the enthalpy of the molecule was calculated as a function of temperature.

To obtain the enthalpy of the impurity gas molecule at 600 K, a zero-point energy (ZPE) and the change in the enthalpy from 0 K to 600 K were added to the energy of the molecule obtained in the geometry optimization calculation, i.e.,

$$H_{X_2(g)}^{600\,K} = E_{X_2(g)}^{DFT} + ZPE + \Delta H^{0\,K-600\,K}_{X_2(g)} \quad \text{. (B6)}$$

B.4. Na-impurity solid compound (Debye model)

In our previous study on the benchmark test for O_2, a phonon vibration calculation was performed with quasi-harmonic approximation (QHA) to evaluate the enthalpy of solid Na_2O at target temperatures.[1] In this study, however, it was found that the QHA fails for solid NaI, probably because of the large anharmonicity in the phonon vibration. Specifically, the Helmholtz energy as a function of volume was incorrectly calculated at high temperatures, leading to a significant overestimation of the volume at the high temperatures. In addition, the QHA calculation is computationally expensive because first-principles calculations are performed several times with accurate numerical settings while changing the lattice constant of the solid. Thus, we considered that it would be inaccurate and inefficient to perform the QHA calculations for every impurity case.

In this study, Debye model was selected as an alternative to the QHA calculation. According to the Debye model, the change in the internal energy of a solid from 0 K to T K, $\Delta U^{0\,K-T\,K}$, is expressed as a function of the temperature T and the Debye temperature T_D of the solid, which is

$$\Delta U^{0\,K-T\,K}(T,T_D) = 9Nk_BT\left(\frac{T}{T_D}\right)^3\int_0^{\frac{T_D}{T}}\frac{x^3}{e^x-1}dx \quad \text{where} \quad x = \frac{\hbar\omega}{k_BT} \quad \text{. (B7)}$$

Here, N is the number of atoms in the solid, k_B is the Boltzmann constant, $\hbar = \frac{h}{2\pi}$ is the Dirac's constant, h is the Planck's constant, and ω is the phonon frequency. The Debye temperature can be calculated from the ZPE of the phonon, which is $\frac{3}{2}\hbar\bar{\omega}$ per atom with an average phonon frequency $\bar{\omega}$ where $\hbar\bar{\omega} = \frac{3}{4}k_B T_D$,[8] and thus,

$$ZPE = \frac{9}{8}k_B T_D \text{. (B8)}$$

To apply the Debye model, the ZPE of Na_iX (s) was evaluated first from the phonon vibration calculation on the geometry optimized structure of Na_iX (s) by using the phonopy code.[9] After the Debye temperature of Na_iX (s) was obtained from the ZPE by using Eq. (B8), the change in the internal energy of Na_iX (s) from 0 K to 600 K was calculated by using Eq. (B7).

At a temperature well below the melting point, the change in the PV value (the product of the system pressure P and volume V) of a solid as a function of temperature should be negligible. Then, the change in the internal energy as a function of temperature, $\Delta U(T)$, can be approximated to the change in the enthalpy, $\Delta H(T)$, from the definition $H = U + PV$. Indeed, the difference between $\Delta U^{0-600\,K}$ and $\Delta H^{0-600\,K}$ was negligible according to the QHA calculation results in Appendix E.4 where U and H were obtained from the following thermodynamic formulas, respectively:

$$U = A + TS,\ H = G + TS \text{ (B9)}$$

where A is the Helmholtz energy, T is temperature, S is entropy, and G is the Gibbs energy.

In summary, $\Delta H(T)$ of Na_iX (s) was estimated from $\Delta U(T)$ of Na_iX (s), which was calculated from the Debye model with the Debye temperature calculated from the ZPE of the phonon. To obtain the enthalpy of Na_iX (s) at 600 K, the ZPE and the change in the enthalpy from 0 K to 600 K was added to the energy of Na_iX (s) obtained in the geometry optimization calculation, i.e.,

$$H^{600\,K}_{Na_iX(s)} = E^{DFT}_{Na_iX(s)} + ZPE + \Delta H^{0\,K-600\,K}_{Na_iX(s)}$$

where

$$\Delta H^{0\,K-T\,K}_{Na_iX(s)} \approx \Delta U^{0\,K-T\,K}_{Na_iX(s)} \approx 9Nk_BT\left(\frac{T}{T_D}\right)^3\int_0^{\frac{T_D}{T}}\frac{x^3}{e^x-1}dx \text{. (B10)}$$

The accuracy of the method using the Debye model is checked in Appendix E.4 through the comparison with the results of QHA calculations and experiments.

C. Pair correlation function (PCF) and coordination number (CN) in impurity-including liquid Na

In Correction-3 and Correction-4, the coordination numbers (CNs) of Na and impurity in Na (*l*) and in Na_iX (*s*) are used to compare the local environment around an impurity atom between Na (*l*) and Na_iX (*s*). The CN, or the number of first-neighboring atoms, is commonly used in solid crystals where the interatomic distance is generally fixed, and the CN in Na_iX (*s*) is simply determined by counting the number of atoms closest to the reference atom. However, to apply this concept to a liquid system, a proper cutoff radius should be determined from the pair correlation function (PCF) for the system.

The PCF describes the variance of the average density of surrounding atoms (e.g., Na), as a function of the radial distance from a reference atom (e.g., impurity). For example, Fig. C shows the PCF of Na-H calculated from the trajectories of atoms in the FPMD simulations of H-including liquid Na. The first peak of the PCF of which the center is located at a distance of 2.20 Å from the H impurity atom corresponds to the first-neighboring Na atoms. The proper cutoff radius for the first-neighboring Na atoms is set as the radial distance at which the PCF becomes the first local minimum, which is 3.48 Å in the case of H impurity. Accordingly, the CN of H with respect to Na is counted as the number of Na atoms located within 3.48 Å from the H atom. Table C lists cutoff radii determined from the PCFs of Na-impurity, which were used to count the CNs of impurities in liquid Na.

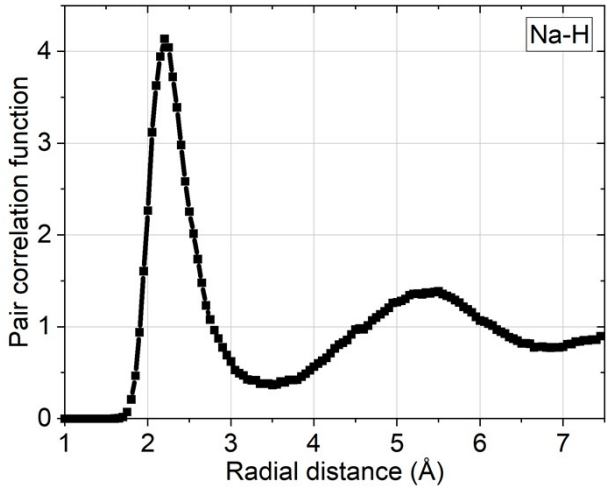

Figure C. PCF of Na-H calculated from FPMD simulation data for H-including liquid Na.

Table C. Cutoff radii to count coordination numbers of impurities in liquid Na, determined from PCFs of Na-impurity.

Impurity	H	N	O	I

Cutoff radius (Å)	3.48	3.50	3.53	4.50

D. Charge-based coordination numbers of impurities in liquid Na

In the present study, the charge-based coordination number (CCN) of impurity was newly defined to count the number of Na-impurity cation-anion bonds in liquid Na in Correction-4. Unlike the conventional CN, the CCN counts only the first-neighboring Na atoms whose charge exceeds a threshold value. This charge threshold for the first-neighboring Na atom was set to +0.2*e*, as mentioned in Sec. 3.4 in the main body. The criterion was established by comprehensively considering the results of the Bader charge analysis,[10] the CCN, and the calculation error in the solution enthalpy, which will be described throughout this section.

The Bader charge analysis was performed on 40 trajectories randomly selected from the FPMD simulation data for each impurity-including liquid Na. The charge distributions of the non-first-neighboring (colored in black) and the first-neighboring (colored in red) Na atoms of the O and I impurity atoms in liquid Na are shown in Fig. D1. For each of the two simulations, marked as #1 and #2 in Fig. D1, 20 trajectories were randomly selected to examine the charge distribution of the Na atoms in the O-including and I-including liquid Na systems.

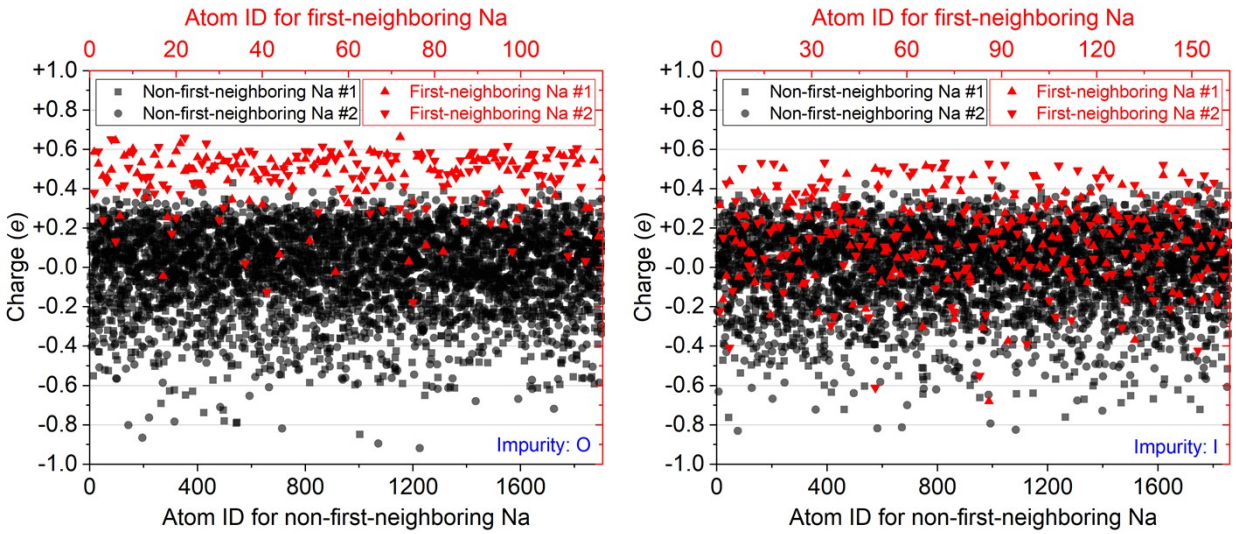

Figure D1. Charge distributions of non-first-neighboring and first-neighboring Na atoms of O impurity (left) and I impurity (right) atoms in liquid Na.

It was observed that the charge distribution of the non-first-neighboring Na atoms was similar regardless of the simulation (whether #1 or #2) and the impurity element (whether O or I). Table D1 shows the mean and standard deviation of these charges, which are all approximately $0 \pm 0.2e$. These results indicate that charge variations in this range occur as deviations in the Bader charge analysis for high-temperature liquids.

In contrast, the first-neighboring Na atoms were observed to have a clearly different charge distribution depending on the impurity. For example, according to Fig. D1 and Table D1, the charge distribution of the first-neighboring Na atoms of the O impurity is relatively concentrated on the positive charge side, with an average of +0.45*e* and with a relatively small standard deviation of 0.15*e*, while that of the I impurity is relatively uniform over various charges, with an average of +0.15*e* and with a relatively large standard deviation of 0.23*e*. This indicates that the interaction between the O impurity and its neighboring Na atoms is relatively ionic compared to the interaction between the I impurity and its neighboring Na atoms.

Table D1. Mean and standard deviation of Na charges in O-including and I-including liquid Na. The data for each case were obtained in two independent FPMD simulations, marked as #1 and #2.

Impurity	O		I	
Simulation	#1	#2	#1	#2
Charge of non-first-neighboring Na atoms of impurity atom (*e*)	+0.01 ± 0.21	+0.01 ± 0.21	+0.00 ± 0.21	+0.00 ± 0.21
Charge of first-neighboring Na atoms of impurity atom (*e*)	+0.46 ± 0.14	+0.44 ± 0.16	+0.15 ± 0.21	+0.16 ± 0.24

Next, the CCNs of the impurities in liquid Na are plotted as a function of the charge threshold in Fig. D2. For example, "charge threshold of +0.2*e*" on the *x*-axis in Fig. D2 means that the CCN was obtained by counting the number of first-neighboring Na atoms of which charges were greater than +0.2*e*. For N and O, the CN and the CCNs with a small charge threshold, e.g., up to +0.3*e*, are relatively similar while the CCN rapidly decreases with a large charge threshold, e.g., +0.4*e* and above, which reflects a relatively concentrated charge distribution on the positive side, as shown in the O case in Fig. D1. In contrast, for H and I, the CCN decreases almost linearly as the charge threshold increases, which reflects a relatively uniform charge distribution, as shown in the I case in Fig. D1.

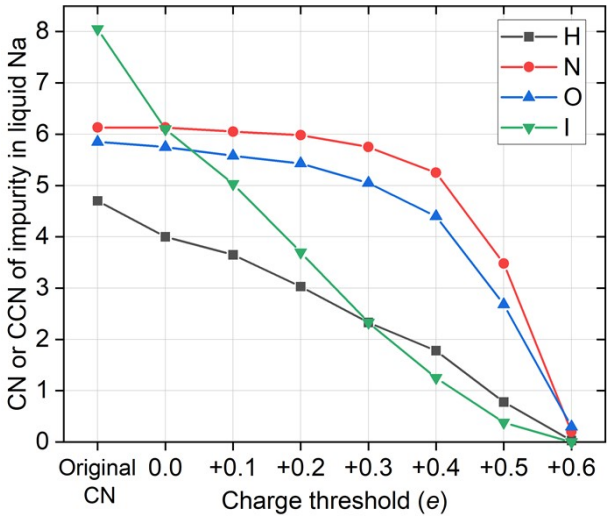

Figure D2. CCNs of impurities in liquid Na as a function of the charge threshold for counting CCN. For example, "charge threshold of +0.2*e*" on the *x*-axis means that the corresponding CCN was obtained by counting the number of first-neighboring Na atoms of which charges were greater than +0.2*e*.

The relatively concentrated charge distribution in the N and O impurity cases indicates that the interaction between the impurity and its neighboring Na atoms is relatively ionic, and the majority of the bonds between the impurity and its first-neighboring Na atoms may be regarded as cation-anion bonds. In contrast, in the H and I impurity cases where the Na-impurity interaction is relatively less ionic, a smaller percentage of the Na-impurity bonds should be regarded as cation-anion bonds. Considering the decreasing trends of the CCNs in Fig. D2, it would be appropriate to set the charge threshold between +0.1*e* and +0.4*e*.

Finally, the relationship between the charge threshold for counting the CCN and the calculation errors in the solution enthalpies of X_2 (*g*) and Na_iX (*s*) was checked, as shown in Fig. D3. Note that the errors in the solution enthalpies of X_2 (*g*) and Na_iX (*s*) are the same when Correction-4 is applied. As discussed in Section 5.3 of the main body, Correction-4 does not reduce the errors in the H_2 (NaH) and the N_2 solution enthalpies. As seen in Fig. D2, the errors in these solution enthalpies does not vary significantly depending on the charge threshold. Thus, it is reasonable to focus on the errors in the O_2 (Na_2O) and I_2 (NaI) solution enthalpies, and it is clearly seen that the charge threshold of +0.2*e* reduces these errors the most.

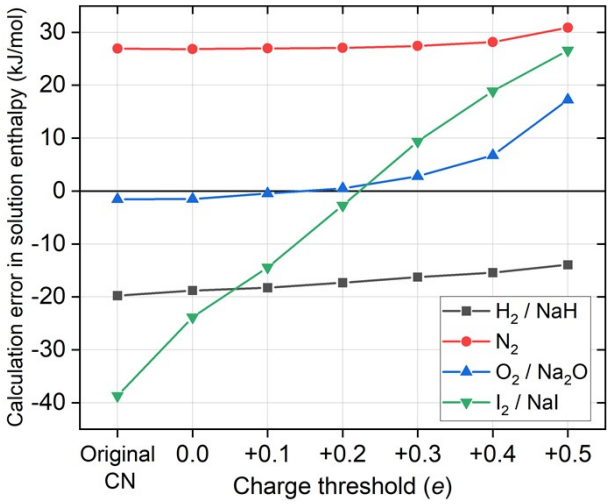

Figure D3. Calculation errors in the solution enthalpies as a function of charge threshold. Note that the calculation errors in the solution enthalpies of X_2 (g) and Na_iX (s) are the same when Correction-4 is applied.

Additionally, according to Table D1, 0.2e is close to the standard deviations of the non-first-neighboring Na atoms in all four impurity cases. This implies that, if a Na atom has a charge greater than +0.2e, it is reasonable to consider that the atom is more likely to be charged mainly from the interaction with the impurity atom, rather than from the interaction with other Na atoms. Thus, by comprehensively analyzing the results from Fig. D1-D3 and Table D1, we decided to set the charge criterion for counting the CCN as a charge greater than +0.2e.

Table D2 compares the CNs and the CCNs of the impurity atoms in liquid Na. In the cases of N and O, the CCN is over 90% of the CN, which means the N and O impurity atoms exchange electrons actively with most of their first-neighboring Na atoms. In contrast, in the cases of H and I, the CCN is about 65% and 48% of the CN, respectively, which means the H and I impurity atoms exchange electrons actively with only some of their first-neighboring Na atoms.

Table D2. CNs and CCNs of impurity atoms in impurity-including liquid Na.

Impurity	H	N	O	I
CN of impurity in liquid Na	4.64	6.07	5.76	7.78
CCN of impurity in liquid Na	3.03	5.98	5.43	3.70

E. Results of the first-principles calculations

E.1. Pure liquid Na

Figure E1 shows the pressure-energy relationship of pure liquid Na, obtained from the FPMD simulations. Because the energy cutoff for plane waves (ENCUT) was set differently depending on the impurity, as mentioned in Section 2.2 of the main body, the relationship was separately obtained from the simulations with the energy cutoff of 300 eV and 400 eV. Each data point in Fig. E1 represents the pressure and energy averaged over three simulations starting with different atomic configurations. Each error bar represents the standard errors of mean (SEMs), which are caused by the thermal fluctuation during each simulation and by the deviation among three simulations.

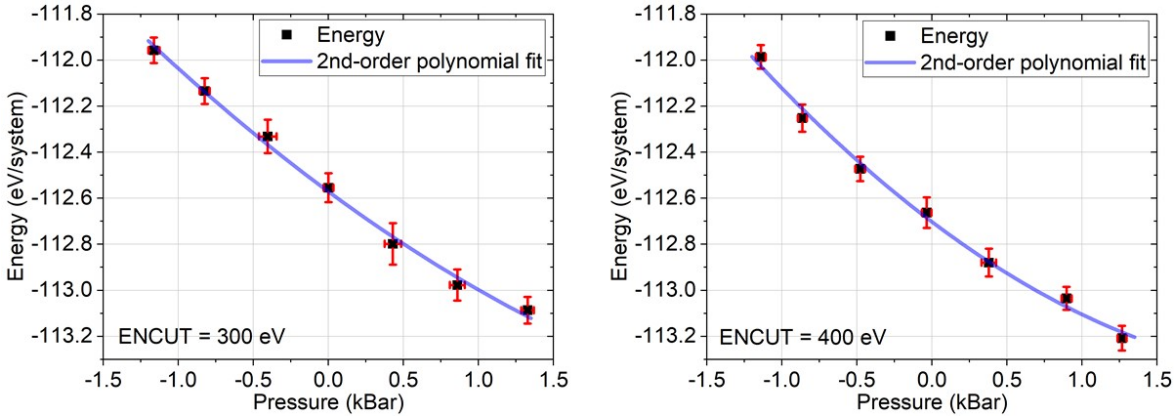

Figure E1. Pressure-energy relationship of pure liquid Na obtained separately from FPMD simulations with energy cutoffs for plane waves (ENCUT) of 300 eV (left) and 400 eV (right).

By fitting the seven data points of different volumes to the second-order polynomial with the error bars considered as weighting factors, the energy at which the pressure becomes zero, or the zero-pressure energy, was estimated as the *y*-intercept of the polynomial. Its standard deviation was numerically estimated by using a Monte Carlo method, assuming that each data point has a normal distribution with the error bars in Fig. E1 being the standard deviations.[1] Finally, the *PV* value was added to the zero-pressure energy to obtain the enthalpy of pure liquid Na at 600 K. Because the zero pressure is virtually equivalent to the atmospheric pressure for simulations of condensed matter, the atmospheric pressure (101325 Pa) was used as the pressure *P* in the *PV* value. The results are summarized in Table E1.

Table E1. Summary of calculation results for enthalpy of pure liquid Na at 600 K separately obtained from FPMD simulations with different ENCUT values.

ENCUT (eV)	300	400
Zero-pressure energy (eV/system)	–112.5708 ± 0.0445	–112.7022 ± 0.0379
PV (eV)	0.0028	0.0028
Enthalpy (eV/system)	–112.5680 ± 0.0445	–112.6994 ± 0.0379

E.2. Impurity-including liquid Na

Table E2 summarizes the results for the FPMD simulations of impurity-including liquid Na. Two 30-ps

simulations starting with different atomic configurations were performed for each impurity. After the initial 5-ps data were discarded as equilibration calculations, the system energy and pressure were averaged over 25 ps for each simulation, which are shown with their SEMs in Table E2. Although the cell constants estimated in 5-ps test simulations to result in the zero pressure were used, the average system pressures were not exactly zero. Thus, by using the pressure-energy relationship of pure liquid Na shown in Fig. E1, the system energies were corrected to the values corresponding to the zero pressure. In the cases of H and I where ENCUT was set to 300 eV, the relationship of pure Na obtained with the 300-eV ENCUT was used. In the cases of N and O where ENCUT was set to 400 eV, the relationship obtained with the 400-eV ENCUT was used. Lastly, similarly to the pure liquid Na case, the PV value was added to the average of the zero-pressure energies to evaluate the enthalpy of impurity-including liquid Na at 600 K.

Table E2. Summary of calculation results for enthalpy of impurity-including liquid Na at 600 K obtained from FPMD simulations for each impurity.

Impurity	H		N		O		I	
Simulation	1	2	1	2	1	2	1	2
Energy E (eV/system)	–114.6788 ± 0.0507	–114.6872 ± 0.0584	–118.9518 ± 0.0406	–118.8753 ± 0.0460	–119.9954 ± 0.0436	–119.8320 ± 0.0413	–114.7152 ± 0.0542	–114.8052 ± 0.0539
Pressure P (kBar)	–0.0804 ± 0.0294	–0.0584 ± 0.0307	0.1854 ± 0.0270	0.1281 ± 0.0296	0.0354 ± 0.0264	–0.1970 ± 0.0251	–0.0644 ± 0.0308	–0.0619 ± 0.0245
Correction in E (eV/system)	–0.0390	–0.0283	+0.0880	+0.0615	+0.0173	–0.1003	–0.0312	–0.0300
Zero-P E (eV/system)	–114.7178 ± 0.0507	–114.7155 ± 0.0584	–118.8637 ± 0.0406	–118.8138 ± 0.0460	–119.9782 ± 0.0436	–119.9323 ± 0.0413	–114.7464 ± 0.0542	–114.8351 ± 0.0539
	–114.7167 ± 0.0547		–118.8388 ± 0.0500		–119.9552 ± 0.0482		–114.7908 ± 0.0699	
PV (eV/system)	0.0028		0.0028		0.0028		0.0028	
Enthalpy (eV/system)	–114.7139 ± 0.0547		–118.8360 ± 0.0500		–119.9524 ± 0.0482		–114.7880 ± 0.0699	

E.3. Impurity gas molecule

Figure E2 shows the potential energy curves of the impurity gas molecules, evaluated from first-principles static calculations. The reference energy level where the potential energy is zero was set as the sum of the energies of two isolated impurity atoms. The binding energy and bond length of the molecule where the potential energy becomes the minimum were determined from the first-principles geometry optimization calculation. Also, the harmonic vibration frequency was evaluated by solving Schrödinger equations of atomic vibrations numerically based on the potential energy curves.[11] The results were compared with experimental data, as shown in Table E3. The binding energies of N_2, O_2, and I_2 were overestimated while that of H_2 was slightly underestimated. The structural and vibrational properties of all four gas molecules were relatively well reproduced.

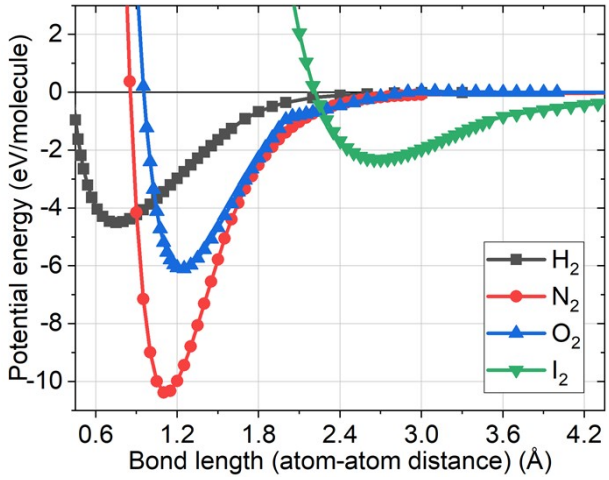

Figure E2. Potential energy curves of impurity gas molecules evaluated from first-principles static calculations.

Table E3. Comparison of calculated quantities for impurity gas molecules with experimental data.

Impurity molecule	H_2		N_2		O_2		I_2	
Calculated or experimental*	Cal.	Exp.	Cal.	Exp.	Cal.	Exp.	Cal.	Exp.
Binding energy** (eV)	4.238	4.478	10.245	9.754	6.007	5.127	2.312	1.539
Bond distance (Å)	0.751	0.741	1.117	1.098	1.234	1.208	2.683	2.666
Harmonic frequency (cm^{-1})	4248	4401	2439	2359	1565	1580	214.1	214.5

* Experimental data: binding energy,[12] bond distance and harmonic frequency.[13]

** Binding energy includes the zero-point vibration energy (ZPE).

From the obtained harmonic vibration frequency, the internal energy of the molecule was calculated under the harmonic approximation as a function of temperature by using Eq. (B4). Subsequently, the enthalpy of the molecule was calculated by using Eq. (B5). Figure E3 shows the results of the vibration analysis for the enthalpies of the impurity molecules as a function of temperature, together with experimental data.[13] Because the vibration frequencies of the impurity molecules were calculated to a reasonably accurate level under the harmonic approximation, the results agree well with the experimental data.[13]

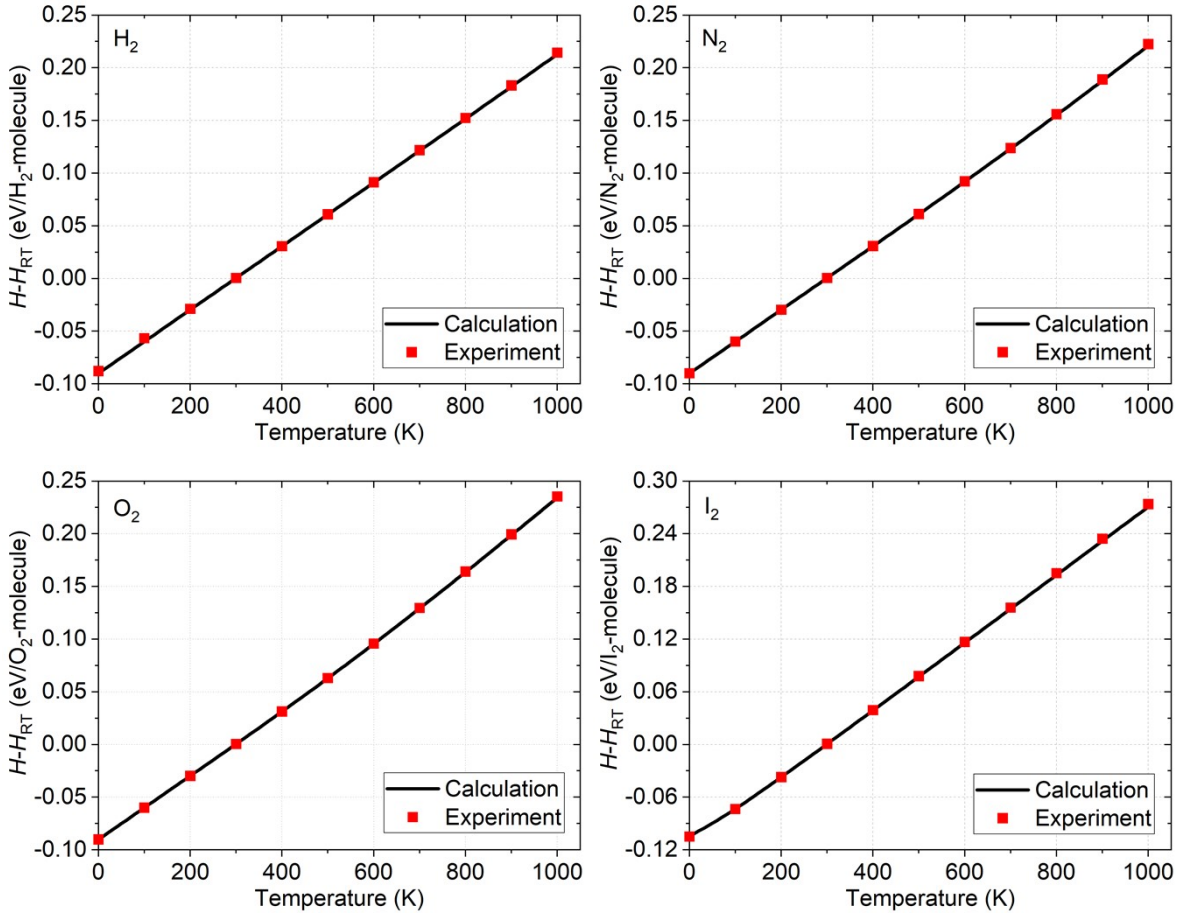

Figure E3. Comparison of change in enthalpy of impurity gas molecule as a function of temperature between calculation result of vibration analysis and experimental data:[14] H_2 (top left), N_2 (top right), O_2 (bottom left), and I_2 (bottom right).

Table E4 lists the calculated quantities for the evaluation of the enthalpies of the impurity gas molecules at 600 K. Specifically, the enthalpy at 600 K, $H_{600\,K}$, was calculated by adding the zero-point vibrational energy (ZPE) and the change in the enthalpy from 0 K to 600 K, $\Delta H_{0-600\,K}$, to the potential energy obtained from the first-principles geometry optimization calculation, $E^{DFT}_{0\,K}$.

Table E4. Calculated quantities for evaluation of enthalpies of impurity gas molecules at 600 K.

Impurity gas molecule	H_2	N_2	O_2	I_2
$E^{DFT}_{0\,K}$ (eV/molecule)	–6.7259	–16.6203	–9.8771	–2.6721
ZPE (eV/molecule)	0.2633	0.1512	0.09704	0.0133
$\Delta H_{0-600\,K}$ (eV/molecule)	0.1810	0.1818	0.1856	0.2205
$H_{600\,K}$ (eV/molecule)	–6.2816	–16.2873	–9.5944	–2.4383

E.4. Na-impurity solid compound

In this study, NaH, Na_2O, and NaI were selected as $Na_iX\,(s)$ because they are the most thermodynamically stable sodium compounds at 600 K for H, O, and I impurities, respectively. In the case of N, two possible $Na_iX\,(s)$ compounds, sodium nitride (Na_3N) and sodium azide (NaN_3), decompose at temperatures below 600 K, and there is no stable form of $Na_iX\,(s)$ at 600 K.[3]

First, to obtain the change in the enthalpy of $Na_iX\,(s)$ as a function of temperature by applying the Debye model, the ZPE of $Na_iX\,(s)$ is needed. To obtain the ZPE, phonon vibration calculations on the geometry optimized structure of $Na_iX\,(s)$ were performed by using the phonopy code[9] with the setting written in Section 2.2 of the main body. Table E5 lists (i) the ZPEs obtained from the phonon vibration calculations and (ii) the Debye temperatures obtained from the ZPEs by using Eq. (B8).

Table E5. ZPEs and Debye temperatures of $Na_iX\,(s)$, obtained from phonon vibration calculations.

$Na_iX\,(s)$	NaH	Na_2O	NaI
ZPE (eV/Na_iX)	0.1623	0.1351	0.0309
Debye temperature (K)	842.9	444.0	160.5

Next, the change in the internal energy of $Na_iX\,(s)$ from 0 K to 600 K was calculated from Eq. (B7) by using the obtained Debye temperature. Table E6 compares (i) the change in the internal energy from 0 K to 600 K, $\Delta U_{0-600\,K}$, calculated from the Debye model, (ii) that calculated from the QHA calculation, (iii) the change in the enthalpy from 0 K to 600 K, $\Delta H_{0-600\,K}$, calculated from the QHA calculation, and (iv) that referred from experimental data.[15] The setting and procedure of the QHA calculation were similar to those for Na_2O in the previous study.[1] The internal energy U and the enthalpy H were obtained from the results of the QHA calculation by using Eq. (B9). The results of the QHA calculation for NaI are not available because the QHA calculation failed for NaI, as mentioned in Appendix B.

Table E6. Comparison between (i) $\Delta U_{0-600\,K}$ calculated from Debye model, (ii) $\Delta U_{0-600\,K}$ and (iii) $\Delta H_{0-600\,K}$ calculated from QHA, and (iv) $\Delta H_{0-600\,K}$ brought from experimental data.[15]

Calculation from \ Solid compound		NaH	Na_2O	NaI
(i) Debye model	$\Delta U_{0-600\,K}$ (kJ/mol)	17.05	33.66	27.04
(ii) QHA		20.02	34.69	N/A*
(iii) QHA	$\Delta H_{0-600\,K}$ (kJ/mol)	20.02	34.69	N/A*
(iv) Experimental		19.69	36.03	28.93

* The QHA calculation failed for NaI, as mentioned in Appendix B.

At temperatures well below the melting point, the change in the PV value of a solid according to the temperature should be negligible. Then, ΔU according to the temperature can be approximated to ΔH considering the definition, $H = U + PV$. Indeed, the difference between $\Delta U_{0-600\,K}$ and $\Delta H_{0-600\,K}$ was negligible for both NaH and Na_2O according to the results of the QHA calculations in Table E6. Thus, $\Delta U_{0-600\,K}$ calculated from the Debye model was directly used to estimate $\Delta H_{0-600\,K}$.

Figure E4 depicts the calculation results of the Debye model for $\Delta U_{0-600\,K}$ of $Na_xX\,(s)$ and compares them with the experimental data for $\Delta H_{0-600\,K}$.[14] According to Table E6 and Fig. E4, the $\Delta U_{0-600\,K}$ of the Debye model underestimates the experimental $\Delta H_{0-600\,K}$ of $Na_xX\,(s)$ only by 2-3 kJ/mol. This level of calculation error is acceptable, considering the computational cost of the Debye model, which is significantly lower than that of the QHA calculation, as the phonon calculation with the Debye model is performed only with one volume.

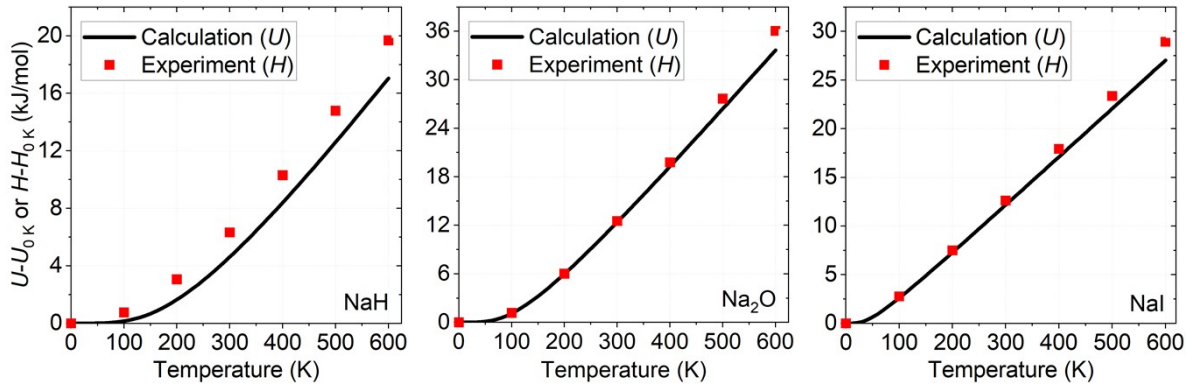

Figure E4. Comparison between calculation results of Debye model for change in internal energy, ΔU, and

experimental data for change in enthalpy, ΔH, from 0 K to 600 K: NaH (left), Na_2O (middle), and NaI (right).

Finally, Table E7 lists the calculated quantities for the evaluation of the enthalpies of Na_iX (s) at 600 K. Specifically, the enthalpy at 600 K, $H_{600\,K}$, was calculated by adding the zero-point vibrational energy (ZPE) and the change in the enthalpy from 0 K to 600 K, $\Delta H_{0-600\,K}$, to the potential energy obtained from the first-principles geometry optimization calculation, $E_{0\,K}^{DFT}$.

Table E7. Calculated quantities for evaluation of enthalpies of Na_iX (s) at 600 K.

Solid compound	NaH	Na_2O	NaI
$E_{0\,K}^{DFT}$ (eV/Na_iX)	–5.1095	–11.3737	–5.4036
ZPE (eV/Na_iX)	0.1623	0.1351	0.0309
$\Delta H_{0-600\,K}$ (eV/Na_iX)	0.2075	0.3595	0.2804
$H_{600\,K}$ (eV/Na_iX)	–4.7397	–10.8791	–5.0923

F. Local structure around an impurity in liquid Na

The strength of the interaction between Na and impurity can be roughly predicted from the local structure around an impurity in liquid Na. One direct method to investigate the local structure is to visualize the trajectories of the FPMD simulation. Figure F1 shows the snapshots of the local structures of Na-impurity during the FPMD simulations of O-including and I-including liquid Na. The interatomic bonds were shown between the impurity atom and its neighboring Na atoms if their distance is less than the cutoff radius, 3.53 Å for O and 4.50 Å for I, which was determined from the Na-impurity PCF mentioned in Appendix C (see Table C). In the snapshots in Fig. F1, six first-neighboring atoms surround the O atom, and seven first-neighboring atoms surround the I atom.

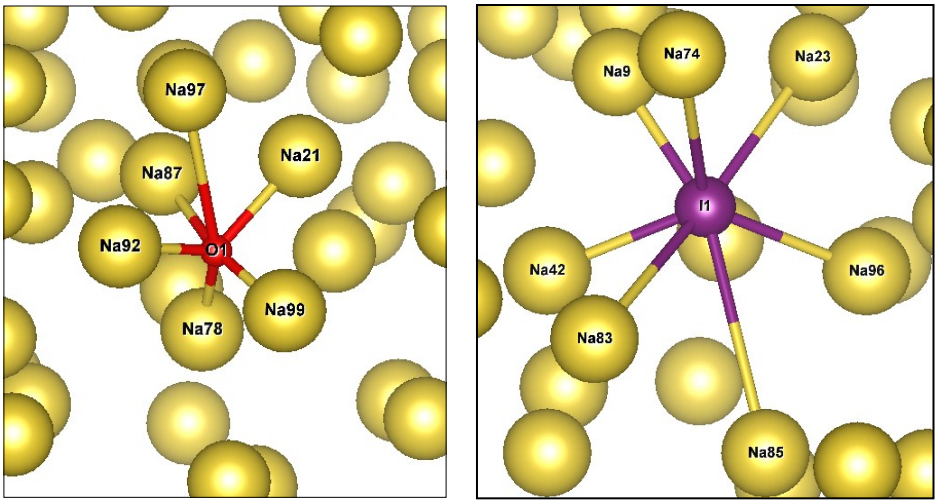

Figure F1. Snapshots of local structures of Na-impurity during FPMD simulations of O-including (left) and I-including (right) liquid Na.

To check the motion of these first-neighboring Na atoms in FPMD trajectories before and after the snapshots in Fig. F1, the change in the distance from the impurity atoms to these atoms over time was calculated, which is shown in Fig. F2. In Fig. F2, the first-neighboring atoms in Fig. F1 are colored to distinguish these atoms from other Na atoms. In the case of O, it was observed that the first-neighboring atoms and the next-neighboring atoms were clearly distinguished based on the cutoff radius (3.53 Å), and the first-neighboring atoms were not changed to other atoms in a short time. This indicates that the local structure of Na-O is relatively fixed like a molecule and the interaction between Na and O is relatively strong. In contrast, in the case of I, it was observed that the distinction between the first-neighboring atoms and the next-neighboring atoms by the cutoff radius (4.50 Å) was relatively less clear than the O impurity case, and the first-neighboring atoms were changed continuously in a relatively short time. This observation indicates that the local structure of Na-I is relatively liquid-like and the interaction between Na and I is relatively weak.

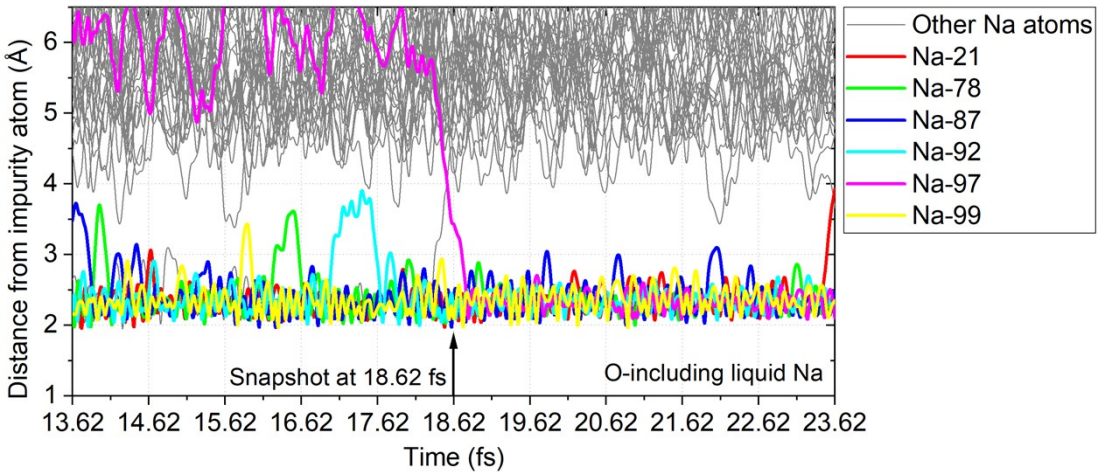

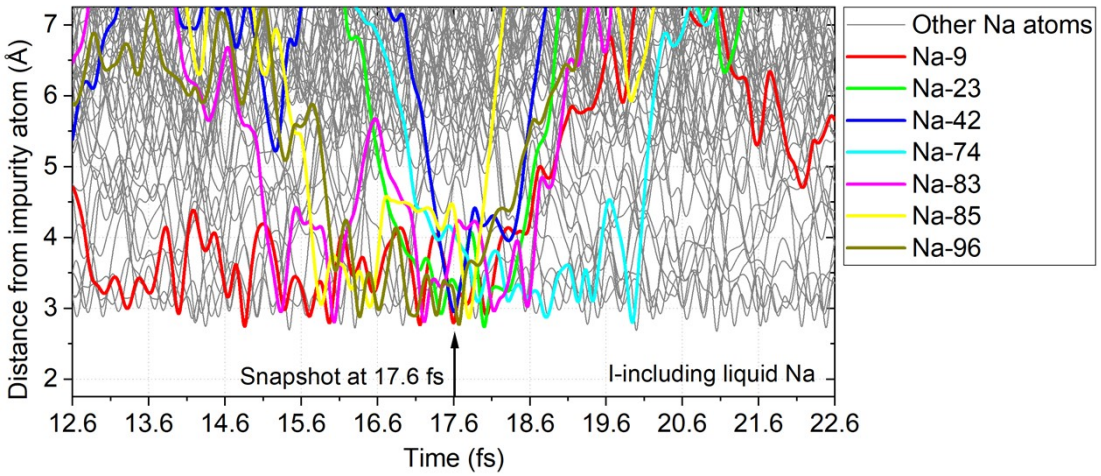

Figure F2. Change in distance from impurity atoms to first-neighboring Na atoms over time for O-including (top) and I-including (bottom) liquid Na. Colored lines are for first-neighboring Na atoms in the snapshots in Fig. F1, and gray lines are for the other Na atoms in the snapshots in Fig. F1.

G. Determination of FERE shifts from calculation errors in formation enthalpies of binary compounds

In Correction-3, to ensure the transferability, the FERE shifts were obtained by minimizing the sum of the squared errors in the formation enthalpies of NaH (*s*), Na_3N (*s*), Na_2O (*s*), Na_2O_2 (*s*), NaI (*s*), LiH (*s*), Li_3N (*s*), Li_2O (*s*), Li_2O_2 (*s*), LiI (*s*), KH (*s*), K_2O (*s*), K_2O_2 (*s*), and KI (*s*) with the least-squares fitting method.

The calculation procedure for the formation enthalpies is as follows. First, the energies of (i) the alkali metals in their solid crystal states, i.e., Na (*s*), Li (*s*), and K (*s*), and (ii) the impurities in their gaseous molecular states, i.e., H_2 (*g*), N_2 (*g*), O_2 (*g*), and I_2 (*g*), were obtained by the geometry optimization calculation using DFT-PBE, as listed in Table G1. Note that the energies obtained by this calculation are of 0 K without zero-point energies (ZPEs). Except for I_2 (*g*), the standard states at RT – the reference temperature of the experimental data for the formation enthalpies – were selected. In the case of I_2, because the van der Waals interactions, which are found in I_2 (*s*) – the standard state of I at RT – are well known to be inappropriately described by common exchange-correlation functionals of the generalized gradient approximation (GGA),[16–18] the energy of I_2 (*g*) was calculated instead. The experimental formation enthalpy of I_2 (*g*) at 0 K, which is the change in the enthalpy from I_2 (*s*) to I_2 (*g*) at 0 K, 65.5 kJ/mol,[14] was subtracted from the energy of I_2 (*g*) to obtain the enthalpy of I_2 (*s*) at 0 K without a ZPE.

Table G1. DFT-PBE geometry optimization calculation results for energies of Na (*s*), Li (*s*), K (*s*), H_2 (*g*), N_2 (*g*), O_2 (*g*), and I_2 (*g*). Note that the energy of I_2 (*s*), –323.3 kJ/mol, was obtained by subtracting the experimental formation enthalpy of I_2 (*g*) at 0 K, 65.5 kJ/mol,[14] which corresponds to the enthalpy of

sublimation at 0 K, from the calculated energy of I_2 (*g*), –257.8 kJ/mol.

Materials	(i) Alkali metals			(ii) Impurities			
	Na (*s*)	Li (*s*)	K (*s*)	H_2 (*g*)	N_2 (*g*)	O_2 (*g*)	I_2 (*s*)
Energy obtained by geometry optimization using DFT-PBE (kJ/mol)	–126.1	–183.3	–99.2	–649.0	–1603.6	–953.0	–323.3

Next, the energies of the 14 binary compounds, composed of one of the alkali metals and one of the impurities, were obtained by the geometry optimization calculation using DFT-PBE, as listed in Table G2. It should be noted that the least-squares fitting is underdetermined if only the hydrides, nitrides, monoxides, and iodides are included in the fitting because the oxidation number of each anion is the same. Accordingly, Na_2O_2 (*s*), Li_2O_2 (*s*), and K_2O_2 (*s*), where the formal charge of O, –1, is different from the formal charge of O in Na_2O (*s*), Li_2O (*s*), K_2O (*s*), and O-including Na (*l*), –2, were additionally included in the fitting, with the confirmation that this inclusion does not degrade the quality of the fitting; Ref.[19] also included these peroxides in the fitting of the FERE shifts. K_3N (*s*) was excluded in the fitting because the experimental data for the formation enthalpy of K_3N (*s*), available only in Ref.[20], were considered inaccurate; the accuracy of the other experimental data in Ref.[20] was not good when compared with Ref.[14]. Indeed, when K_3N (*s*) was included, the quality of the fit, which was represented by the R-square value and the standard error, was significantly worsened.

Table G2. DFT-PBE geometry optimization calculation results for energies of 14 binary compounds, composed of one of alkali metals, i.e., Na, Li, or K, and one of impurities, i.e., H, N, O, or I. K_3N (*s*) was not included in the fitting because its experimental data, only available in Ref.[20], was considered inaccurate.

Anion / Cation	H_2 (*g*)	N_2 (*g*)	O_2 (*g*)		I_2 (*s*)
Na (*s*)	NaH (*s*) –492.6	Na_3N (*s*) –1105.0	Na_2O (*s*) –1098.4	Na_2O_2 (*s*) –1647.9	NaI (*s*) –521.4
Li (*s*)	LiH (*s*) –588.6	Li_3N (*s*) –1505.8	Li_2O (*s*) –1384.9	Li_2O_2 (*s*) –1878.8	LiI (*s*) –561.7
K (*s*)	KH (*s*) –462.1	K_3N (*s*) -	K_2O (*s*) –966.9	K_2O_2 (*s*) –1555.1	KI (*s*) –533.7

From the calculation results in Tables G1 and G2 and the calculated energies of the impurity gas molecules, shown as $E_{0\,K}^{DFT}$ in Table E4, the formation enthalpies of the 14 binary compounds, at 0 K without ZPEs, were evaluated by subtracting the sum of the energies of the constituents from the energy of a binary compound. The results are listed in Table G3, with the experimental data at RT. It is acceptable to compare the calculation results with the experimental data at RT; as mentioned in Ref.[19,21], the error due to the difference in the reference temperature is typically less than 0.03 eV/atom, which is not significant compared to the error in the formation enthalpies after the FERE correction. Also, because the zero-point vibrational motion is implicitly included in the experimental data for the formation enthalpies, it is also implicitly included in the FERE shifts although the energies obtained by the DFT geometry optimization calculations do not include ZPEs.

Table G3. DFT-PBE calculation results for formation enthalpies of 14 binary compounds at 0 K, compared with experimental data at RT (Na_3N: [22], others: [14]).

Cation \ Anion	H_2 (*g*)	N_2 (*g*)	O_2 (*g*)		I_2 (*s*)
Na (*s*)	NaH (*s*) Cal: –42.0 Exp: –56.4	Na_3N (*s*) Cal: +75.2 Exp: +64.0	Na_2O (*s*) Cal: –369.7 Exp: –418.0	Na_2O_2 (*s*) Cal: –442.7 Exp: –513.2	NaI (*s*) Cal: –233.6 Exp: –287.9
Li (*s*)	LiH (*s*) Cal: –80.8 Exp: –90.6	Li_3N (*s*) Cal: –154.0 Exp: –164.6	Li_2O (*s*) Cal: –541.7 Exp: –598.7	Li_2O_2 (*s*) Cal: –559.2 Exp: –632.6	LiI (*s*) Cal: –216.8 Exp: –270.1
K (*s*)	KH (*s*) Cal: –38.4 Exp: –57.8	K_3N (*s*) -	K_2O (*s*) Cal: –292.1 Exp: –363.2	K_2O_2 (*s*) Cal: –403.8 Exp: –495.8	KI (*s*) Cal: –272.9 Exp: –327.9

The calculation errors in the formation enthalpies of the 14 binary compounds, defined as "(calculated value) – (experimental value)", are shown as "Before FERE" in Fig. G. By setting the calculation errors as dependent variables and the stoichiometric coefficients of the binary compounds as independent variables, the FERE shifts of the seven elements, i.e., Na, Li, K, H, N, O, and I, were obtained by the least-squares fitting. The results for the FERE shifts are listed in Table G4. The R-square value and the standard error of the data after the fit were 0.9977 and 3.61 kJ/mol, respectively. The errors in the formation enthalpies after applying the FERE correction with the obtained FERE shifts are depicted as "After FERE" in Fig. G. It is clearly seen that the errors were significantly decreased after the FERE correction, which means that the FERE correction was successfully applied.

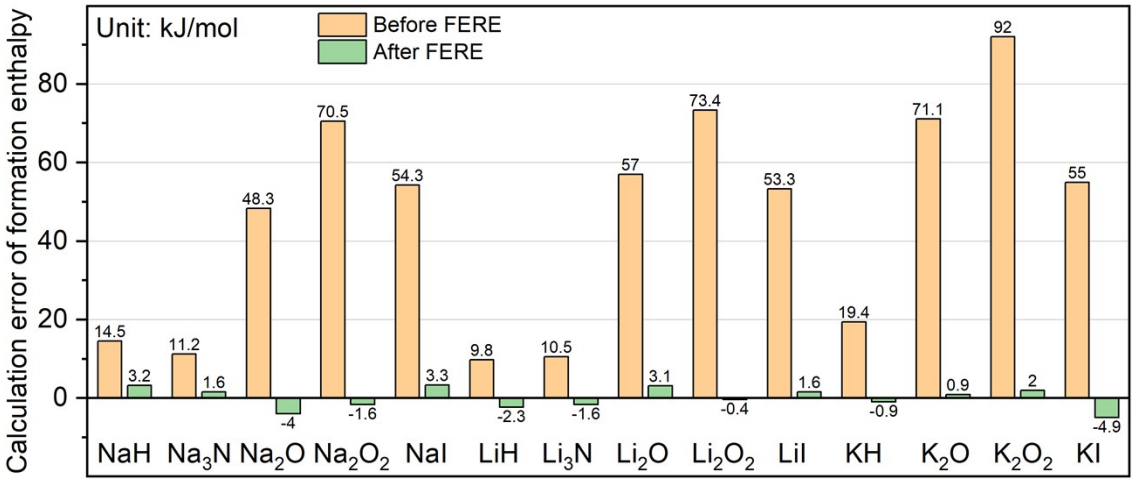

Fig. G. Calculation errors in formation enthalpies of 14 binary compounds before and after FERE correction was applied. Here, (calculation error) = (calculated value with/without FERE correction at 0 K) – (experimental value at RT).

Table G4. FERE shifts determined from calculation errors in formation enthalpies of 14 binary compounds by least-squares fitting method, compared with FERE shifts presented in Ref.[19]. The FERE shifts of H and I are not available in Ref.[19].

Element	FERE shift (kJ/mol)	
	Obtained in this study	Obtained in Ref.[19]
Na	+16.2	+16.4
Li	+17.0	+20.3
K	+25.2	+27.0
H	–4.92	N/A
N	–39.0	–19.3
O	+19.9	+22.2
I	+34.7	N/A

The FERE shifts proposed in Ref.[19] are also listed in Table G4. The FERE shifts of Na, Li, K, and O obtained in this study are comparable to those in Ref.[19] while the FERE shift of N obtained in this study, –39.0 kJ/mol, is quite different from that in Ref.[19], –19.3 kJ/mol. This difference should be mainly because in the present study, only Na_3N (*s*) and Li_3N (*s*) were considered in determining the FERE shift of N, whereas in Ref.[19], 14 binary compounds containing N as a constituent element were considered. The constituents of the 14 binary compounds in Ref.[19] include not only alkali metals but also alkaline earth metals and transition metals. Thus, the FERE shift of N obtained in the present study should be more specialized and is expected to show higher accuracy in the environment where an alkali metal and N interact with each other, while that proposed in Ref.[19] can be applied to a wider variety of environments with fair accuracy.

Lastly, Table G5 shows the calculation errors in the formation enthalpies of Na_tX (*s*) at 600 K before and after the FERE correction was applied. Although the temperature in both the calculated and experimental data[14] were changed to 600 K, except for the experimental data for Na_3N where only the data at RT is available,[22] the FERE correction was successfully applied, resulting in the error of a few kJ/mol after the correction.

Table G5. Calculation errors in formation enthalpies of Na_iX (s) at 600 K before and after FERE correction was applied. Here, (calculation errors) = (calculated values before/after FERE correction at 600 K) – (experimental values at RT for Na_3N[22], at 600 K for the others[14]).

Na_iX (s)	Calculation error in formation enthalpy at 600 K (kJ/mol)	
	Before FERE	After FERE
NaH	9.1	–2.2
Na_3N	9.1	–0.5
Na_2O	48.8	–3.5
NaI	52.9	2.0

H. Contribution of first-neighboring Na of impurity in liquid Na to calculation error in Correction-3

In Correction-3, the contribution of the first-neighboring Na atoms of the impurity atom in liquid Na to the error in the enthalpy of impurity-including liquid Na was neglected, as shown in Eq. (4) in the main body. This was because the contribution was expected to be much smaller than that of the impurity atom, although not zero, as each first-neighboring Na atom was mostly surrounded by other Na atoms. To check if partially considering the contribution of the first-neighboring Na atoms to the error in the enthalpy of impurity-including liquid Na, that is, a partial inclusion of the FERE shift of Na, improves the accuracy of Correction-3, Eq. (4) in the main body was modified as follows:

[Original] (Correction to impurity-including Na (l)) = $-\delta_X^{FERE}$, (4)

[Modified] (Correction to impurity-including Na (l)) = $-\left(\alpha i\delta_{Na}^{FERE}+\delta_X^{FERE}\right)$, (H1)

where α is a contribution factor of the first-neighboring Na atoms to the error in the enthalpy of impurity-including liquid Na, ranging from 0 to 1. If $\alpha = 0$, there is no contribution from the first-neighboring Na atoms, which is the case of the original Eq. (4) in the main body. If $\alpha = 1$, the contribution is the same as that of the Na atoms in solid compounds. The N impurity case was excluded in the test because Correction-3 cannot be applied due to the different oxidation number of N in liquid Na (–3) from that in solid compounds (–2), as mentioned in the main body.

Figure H1 shows the error in the solution enthalpy after the correction using Eq. (R1), according to the value of α. It is observed that, with a partial consideration of the Na term, the error in the O_2 (g) and Na_2O (s) solution enthalpies does become smaller (e.g., when α~0.4 or α~0.5), whereas the error in the other solution enthalpies rather becomes larger. It should be noted that even without considering the Na term ($\alpha = 0$), Correction-3 decreases the error in the O_2 (g) solution enthalpy from 33.6 kJ/mol (before correction) to 13.7 kJ/mol (after original Correction-3B), as shown in Table 8 in the main body. This test results indicate that the consideration of the Na term does not necessarily improve Correction-3. Besides, even if it does improve Correction-3, the reduction in the error is not expected to be significant. It is also difficult to determine an appropriate value of α for general cases. Thus, it is reasonable to neglect the contribution of the first-neighboring Na atoms when correcting the enthalpy of impurity-including liquid Na by Correction-3.

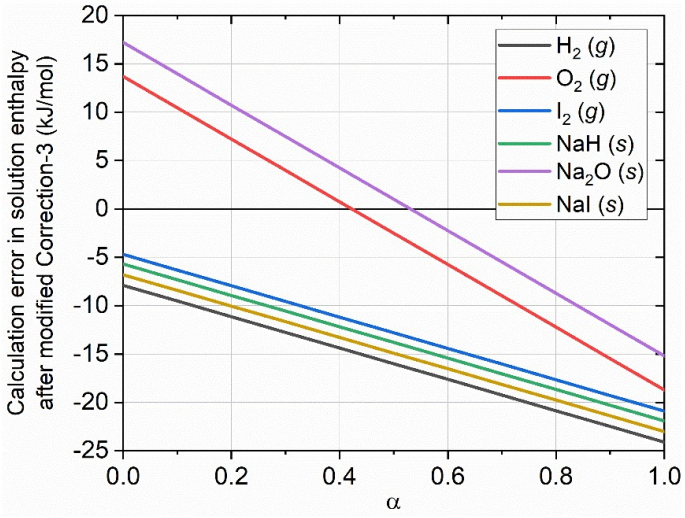

Fig. H1 Calculation error in solution enthalpy after modified Correction-3 using Eq. (H1), according to value of α in Eq. (H1).

I. Possible increase in the calculation error in the solution enthalpies by Correction-4

In this Appendix, the possible increase in the calculation error in the X_2 (g) solution enthalpy by Correction-4 is further analyzed. Figure I1 summarizes the assumptions in Correction-4 and the observations from the results of applying Correction-4, which are discussed in Section 5.3 of the main body. There are four types of calculation errors used in this analysis, which are referred to E_1, E_2, E_3, and E_4 as shown in Fig. I1. One observation was that the difference between the calculation errors in the formation enthalpy of Na_iX (s), E_1, and the X_2 (g) solution enthalpy, E_3, was within 30 kJ/mol for the four tested impurities, namely, $|E_3 - E_1| < 30$ kJ/mol, according to Fig. 6 of the main body. This difference can be expressed as $|\Delta H_2 - \Delta H_3|$ using the notations in Fig. 3 of the main body, and thus is equal to the absolute value of the uncorrected error in the Na_iX (s) solution enthalpy (see Table 9 of the main body).

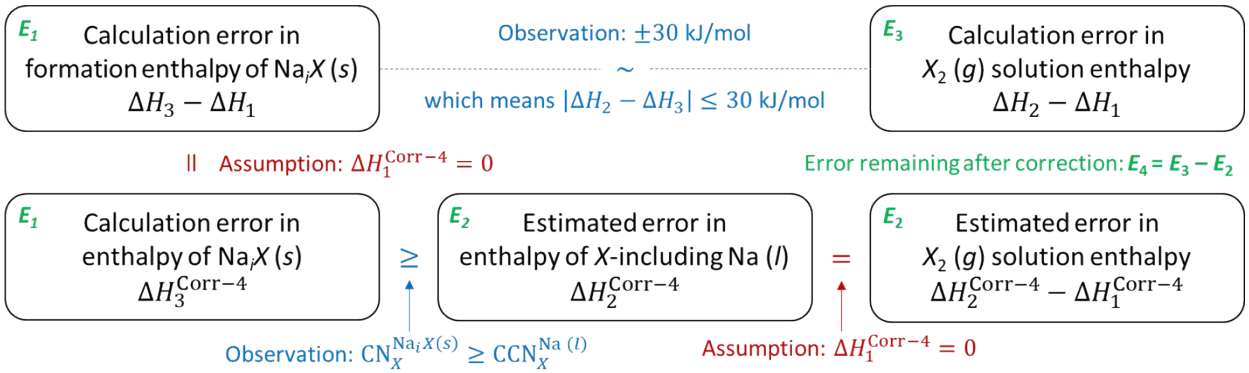

Figure I1. Assumptions in Correction-4 and observations from results of applying Correction-4.

We first limit our discussion to the case where $E_1 \geq 0$, which brings $0 \leq E_2 \leq E_1$, because this condition was achieved for the four tested impurities. The generality of the argument is not degraded due to this condition because it can be easily extended to the case of $E_1 < 0$. For a given range of E_1, possible ranges of E_2, E_3, and E_4 can be estimated based on the assumptions and observations in Fig. I1. If $E_1 \geq 30$ kJ/mol, from the observed relationship between E_1 and E_3, namely, $|E_3 - E_1| < 30$ kJ/mol, the possible range of E_3 can be categorized into two: (i) $E_1 \leq E_3 \leq E_1 + 30$ and (ii) $E_1 - 30 \leq E_3 < E_1$ (unit: kJ/mol), as depicted in the upper left and upper right of Fig. I2, respectively. Comparing E_3 and E_4, which are the calculation errors in the X_2 (g) solution enthalpy without correction and with Correction-4, respectively, the error always decreases by Correction-4 in the case of (i) because $0 \leq E_4 = E_3 - E_2 \leq E_3$ is satisfied, whereas the error may increase in the case of (ii). Specifically, the error may increase up to 30 kJ/mol if $E_3 < -E_4$, and thus, if $E_2 > 2E_3$. Similarly, if $0 \leq E_1 < 30$ kJ/mol, comparing E_3 and E_4 for the possible ranges of E_3, shown as (iii) and (iv) in the lower left and lower right of Fig. I2, respectively, the error always decreases by Correction-4 in the case of (iii), whereas the error may increase in the case of (iv). As in the case of (ii), the error may increase up to 30 kJ/mol if $E_2 > 2E_3$.

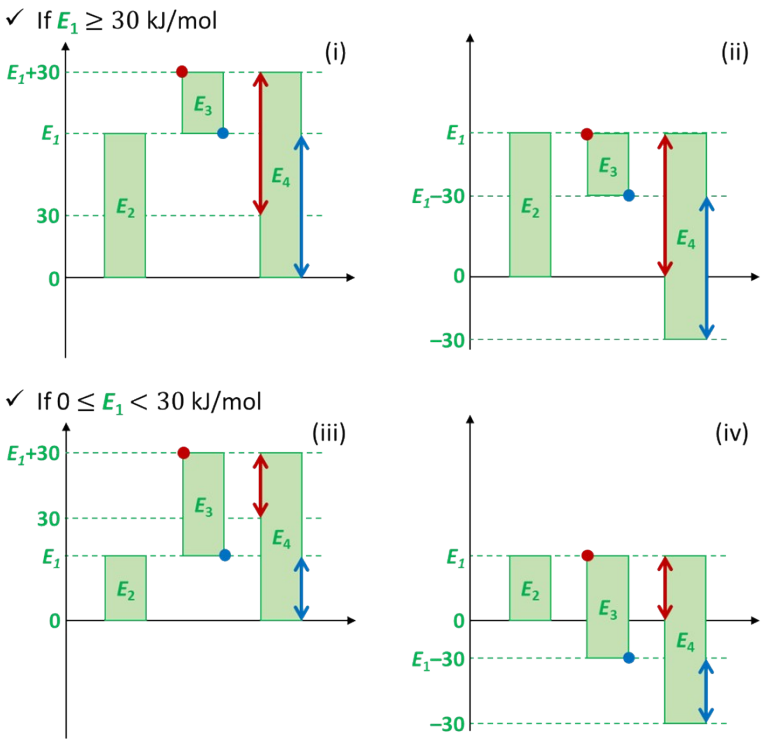

Figure I2. Analysis on possible ranges of E_2, E_3, and E_4 according to two ranges of E_1, $E_1 \geq 30$ kJ/mol (top: (i) and (ii)) and $0 \leq E_1 < 30$ kJ/mol (bottom: (iii) and (iv)). The red and blue dots represent the maximum and minimum values of E_3 given by $|E_3 - E_1| < 30$ kJ/mol, respectively, and the red and blue arrows

represent the expected range of E_4 in each case.

The analysis can be extended to the general value α of the difference between E_1 and E_3, as shown in Fig. I3. For all ranges of E_1, comparing E_3 and E_4, the calculation error in the X_2 (g) solution enthalpy always decreases by Correction-4 when $|E_3| > |E_1|$ whereas the error may increase when $|E_3| < |E_1|$. Specifically, the error may increase up to α if $E_2 > 2E_3$ $(E_1 > 0)$ or if $E_2 < 2E_3$ $(E_1 < 0)$. Because α corresponds to the absolute value of the uncorrected error in the Na_iX (s) solution enthalpy, it means that the maximum value of the possible error in the solution enthalpies after Correction-4 is applied is the absolute value of the uncorrected calculation error in the Na_iX (s) solution enthalpy. Thus, the use of Correction-4 is basically beneficial.

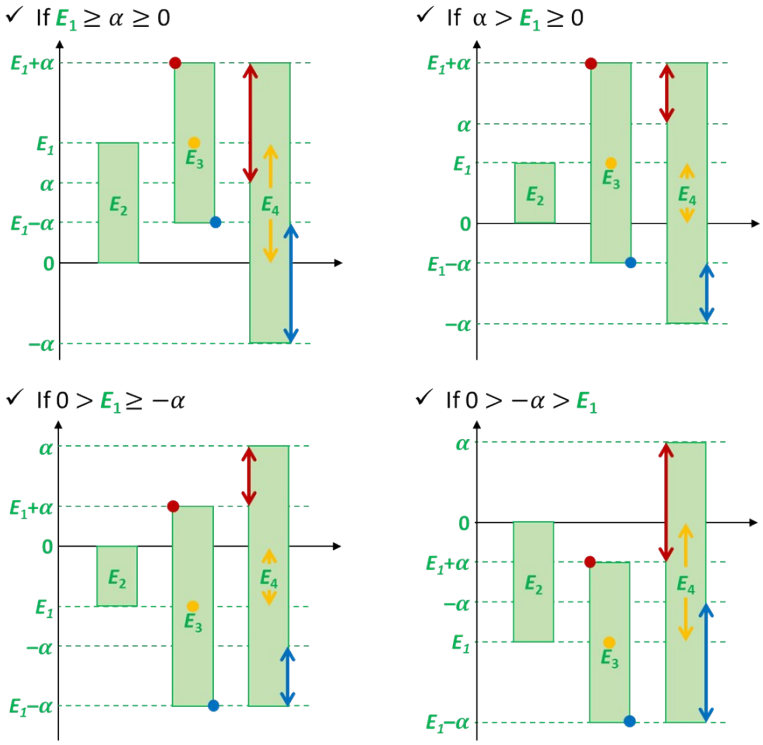

Figure I3. Analysis on possible ranges of E_2, E_3, and E_4 according to ranges of E_1, for general value α of the difference between E_1 and E_3. The red, yellow, and blue dots represent the maximum, median (=E_1), and minimum values of E_3 given by $|E_3 - E_1| < \alpha$, respectively, and the red, yellow, and blue arrows represent the expected range of E_4 in each case.

The calculation errors in the X_2 (g) and Na_iX (s) solution enthalpies become the same by Correction-4. Thus, if the absolute value of the calculation error in the X_2 (g) solution enthalpy is lower than the absolute value of the calculation error in the Na_iX (s) solution enthalpy before the correction is applied, the former may increase by Correction-4, up to at most the latter. This was the case for the H impurity in liquid Na, although

the increase in the error was not large.

References

(1) Gil, J.; Oda, T. Solution Enthalpy Calculation for Impurity in Liquid Metal by First-Principles Calculations: A Benchmark Test for Oxygen Impurity in Liquid Sodium. *J. Chem. Phys.* **2020**, *152* (15), 154503. https://doi.org/10.1063/1.5136324.

(2) Allred, A. L. Electronegativity Values from Thermochemical Data. *J. Inorg. Nucl. Chem.* **1961**, *17* (3–4), 215–221. https://doi.org/10.1016/0022-1902(61)80142-5.

(3) Borgstedt, H. U.; Guminski, C.; Borgstedt, H. U.; Guminski, C. IUPAC-NIST Solubility Data Series. 75. Nonmetals in Liquid Alkali Metals. *J. Phys. Chem. Ref. Data* **2001**, *30* (4), 835–1158. https://doi.org/10.1063/1.1391426.

(4) Han, J. H.; Oda, T. Performance of Exchange-Correlation Functionals in Density Functional Theory Calculations for Liquid Metal: A Benchmark Test for Sodium. *J. Chem. Phys.* **2018**, *148* (14). https://doi.org/10.1063/1.5017198.

(5) Gil, J.; Oda, T. Structural and Chemical Analysis of Second-Row Impurities in Liquid Lead–Bismuth Eutectic by First-Principles Molecular Dynamics. *Phys. Chem. Chem. Phys.* **2018**, *20* (48), 30480–30491. https://doi.org/10.1039/C8CP06019C.

(6) Nosé, S. A Unified Formulation of the Constant Temperature Molecular Dynamics Methods. *J. Chem. Phys.* **1984**, *81* (1), 511–519. https://doi.org/10.1063/1.447334.

(7) McQuarrie, D. A.; Simon, J. D. *Physical Chemistry: A Molecular Approach*; University Science Books: Sausalito, California, 1997.

(8) Alchagirov, A. B.; Perdew, J. P.; Boettger, J. C.; Albers, R. C.; Fiolhais, C. Energy and Pressure versus Volume: Equations of State Motivated by the Stabilized Jellium Model. *Phys. Rev. B* **2001**, *63* (22), 224115. https://doi.org/10.1103/PhysRevB.63.224115.

(9) Togo, A.; Tanaka, I. First Principles Phonon Calculations in Materials Science. *Scr. Mater.* **2015**, *108*, 1–5. https://doi.org/10.1016/j.scriptamat.2015.07.021.

(10) Tang, W.; Sanville, E.; Henkelman, G. A Grid-Based Bader Analysis Algorithm without Lattice Bias. *J. Phys. Condens. Matter* **2009**, *21* (8). https://doi.org/10.1088/0953-8984/21/8/084204.

(11) Lindberg, B. A New Efficient Method for Calculation of Energy Eigenvalues and Eigenstates of the One-Dimensional Schrödinger Equation. *J. Chem. Phys.* **1988**, *88* (6), 3805–3810.

https://doi.org/10.1063/1.453880.

(12) Luo, Y.-R.; Kerr., J. A. Bond Dissociation Energies. In *CRC Handbook of Chemistry and Physics*; CRC Press: Boca Raton, 2012; p 89.

(13) Linstrom, P. J.; Mallard, W. G. *NIST Chemistry WebBook, NIST Standard Reference Database Number 69*; National Institute of Standards and Technology: Gaithersburg, MD 20899, 2019. https://doi.org/10.18434/T4D303.

(14) Chase, M. W. NIST-JANAF Thermochemical Tables, 4th Ed. J. Phys. Chem. Ref. Data. 1998, Monograph 9(Part I and Part II). *J. Phys. Chem. Ref. Data* **1998**, *Monograph*, Part I&II. https://doi.org/10.18434/t42s31.

(15) Chase, Jr., M. W. NIST-JANAF Thermochemical Tables. *J. Phys. Chem. Ref. Data Monogr.* **1998**, *9*, 1–1951.

(16) Perdew, J.; Chevary, J.; Vosko, S.; Jackson, K.; Pederson, M.; Singh, D.; Fiolhais, C. Atoms, Molecules, Solids, and Surfaces: Applications of the Generalized Gradient Approximation for Exchange and Correlation. *Phys. Rev. B* **1992**, *46* (11), 6671–6687. https://doi.org/10.1103/PhysRevB.48.4978.2.

(17) Grimme, S. Semiempirical GGA-Type Density Functional Constructed with a Long-Range Dispersion Correction. *J. Comput. Chem.* **2006**, *27* (15), 1787–1799. https://doi.org/10.1002/jcc.20495.

(18) Chiter, F.; Nguyen, V. B.; Tarrat, N.; Benoit, M.; Tang, H.; Lacaze-Dufaure, C. Effect of van Der Waals Corrections on DFT-Computed Metallic Surface Properties. *Mater. Res. Express* **2016**, *3* (4), 046501. https://doi.org/10.1088/2053-1591/3/4/046501.

(19) Stevanović, V.; Lany, S.; Zhang, X.; Zunger, A. Correcting Density Functional Theory for Accurate Predictions of Compound Enthalpies of Formation: Fitted Elemental-Phase Reference Energies. *Phys. Rev. B* **2012**, *85* (11), 115104. https://doi.org/10.1103/PhysRevB.85.115104.

(20) Moody, G. J.; Thomas, J. D. R. Alkali Metal Nitrides. *J. Chem. Educ.* **1966**, *43* (4), 205. https://doi.org/10.1021/ed043p205.

(21) Lany, S. Semiconductor Thermochemistry in Density Functional Calculations. *Phys. Rev. B* **2008**, *78* (24), 245207. https://doi.org/10.1103/PhysRevB.78.245207.

(22) Vajenine, G. V. Plasma-Assisted Synthesis and Properties of Na 3 N †. *Inorg. Chem.* **2007**, *46* (13), 5146–5148. https://doi.org/10.1021/ic700406q.